Journal of
Polymer Materials

Tech Science Press

http://doi.org/10.32604/jpm.2026.082700

ARTICLE

Particle-Reinforced High-Performance Low-Cost Adhesive for Underwater Applications

Yuanchen Zhang[1] and Linfeng Wang[1,2,*]

[1]College of Mechanical & Electrical Engineering, Nanjing University of Aeronautics and Astronautics, Nanjing, China
[2]Jiangsu Key Laboratory of Bionic Materials and Equipment, College of Mechanical and Electrical Engineering, Nanjing University of Aeronautics and Astronautics, Nanjing, China
*Corresponding Author: Linfeng Wang. Email: wanglf@nuaa.edu.cn

Received: 20 March 2026; Accepted: 05 June 2026; Published: 24 September 2026

ABSTRACT: Underwater adhesives serve as essential functional materials with extensive applications in underwater robotic operations, submarine pipeline installation and maintenance, maritime defense projects, and marine engineering infrastructure. However, the construction of robust and reliable underwater bonding interfaces is severely constrained by substrate surface hydration layers and limited interfacial interaction strength, which has become a core bottleneck restricting the development of high-performance underwater adhesives. Herein, we use *in situ* polymerization and particle reinforcement to enhance adhesion strength: An underwater adhesive is prepared by reacting bis(3-aminopropyl)-terminated polydimethylsiloxane with hexamethylene diisocyanate in the presence of $Ca(OH)_2$, which acts as a precursor of reinforcing $CaCO_3$ particles. Such particle reinforcement effectively hinders crack propagation and enhances structural integrity, which can significantly enhance the bonding strength. The adhesive is fully underwater-curable, demonstrates strong reliable adhesion to diverse substrates including iron, glass, polyethylene terephthalate (PET), and polytetrafluoroethylene (PTFE), and complies with general application requirements. Among the tested substrates, polyethylene terephthalate is bonded most strongly, with its maximum underwater adhesion strength reaching 817 kPa. Furthermore, Rheological characterizations validate its favorable processing stability and tunable viscoelastic properties. Thus, this work provides important theoretical and practical insights for the development of high-performance underwater adhesives, and exhibits promising application prospects in marine engineering and underwater equipment fields.

KEYWORDS: Underwater adhesion; particle-reinforced; adhesion mechanism; adhesion testing

1 Introduction

Underwater adhesives have a broad application scope exemplified by their frequent use in the fixation and maintenance of underwater robots, submarine pipelines, and underwater ships [1–4] and rely on electrostatic and van der Waals forces, hydrophobic interactions, metal coordination, hydrogen bonds, and other interactions [5–8]. In underwater settings, molecular-level adhesive–substrate bridging is hindered by the formation of a hydration layer on the substrate surface [3,9,10]. Hence, the elimination of this layer is important for underwater adhesive design.

The problem of hydration layer formation can be addressed in numerous ways, e.g., dopamine-containing molecules were used to simulate the natural underwater adhesion mechanism of mussels and thus develop high-performance underwater adhesives [6,11–14]. Inspired by starfish tube feet, researchers

from Seoul National University of Science and Technology developed a temporary adhesive with underwater robot–like functions, e.g., underwater rock manipulation [15]. The introduction of hydrophobic alkyl or fluorocarbon groups into the polymer chains of adhesives was reported to markedly enhance their hydrophobicity and thus hinder adhesion interface–water contact and increase adhesion strength [16–18]. Polymers can also be grafted with functional groups absorbing some water molecules to react underwater while repelling others [3]. Such polymers avoid hydration layer–related limitations and engage in various interactions (e.g., covalent and hydrogen bonding, hydrophobic interactions, and metal coordination) with substrates, achieving stable and strong underwater adhesion.

However, current underwater adhesives suffer from high cost, insufficient adhesion strength, and/or preparation difficulty. To address these problems, we herein prepare a low-cost high-strength underwater adhesive by reacting bis(3-aminopropyl)-terminated polydimethylsiloxane (PDMS) with hexamethylene diisocyanate (HDI) in the presence of $Ca(OH)_2$. The materials employed for the adhesive preparation are commonly and cheap chemical commodities. Their costs are substantially lower than those of biologically extracted or bioinspired materials typically employed in underwater adhesives. In addition, this adhesive is fully curable in water and strongly and stably adheres to numerous substrates in underwater settings, exploiting the synergistic combination of physical forces (e.g., covalent crosslinking and hydrogen bonding) and particle reinforcement [19]. The results of adhesion performance tests and rheological property analyses provide theoretical and practical guidance for further research on underwater adhesives for engineering applications.

Statement of Novelty

This study successfully developed a novel underwater adhesive by facilitating the reaction between bis(3-aminopropyl) terminated polydimethylsiloxane (PDMS) and hexamethylene diisocyanate (HDI), while incorporating $Ca(OH)_2$ to generate particles during the adhesive preparation process, thereby achieving particle reinforcement. During the preparation of this adhesive, $Ca(OH)_2$ will react with the CO_2 produced in the reaction to form $CaCO_3$ particles, enhancing the adhesion strength of the adhesive. This adhesive can be fully cured underwater and demonstrates excellent adhesion ability. This study explored the possibility of using *in-situ* polymerization and particle reinforcement to enhance the adhesion strength of adhesives, providing important insights that are both practical and theoretically significant for the future development of underwater adhesives with stronger adhesion performance.

2 Materials and Methods

2.1 Materials

HDI (99%) was purchased from Shanghai Macklin Biochemical Technology Co., Ltd. (Shanghai, China). Bis(3-aminopropyl)-terminated PDMS (Mw ≈ 3000) was purchased from Gelest, Inc. (Morrisville, USA). Tetrahydrofuran (THF, 99.5%) was purchased from Sinopharm Chemical Reagent Co., Ltd. (Shanghai, China). All reagents were used as received without further purification.

2.2 Preparation of the Adhesive

First, 0.1056 g of $Ca(OH)_2$ was completely dissolved in 3.5 g of THF. Then, 5 g PDMS (1.67 mmol) were added to the $Ca(OH)_2$/THF solution. After that, 0.28 g HDI (1.67 mmol) was dropwise added in the mixture, followed by 30 min of ultrasonication. Unless otherwise stated, the molar ratios of amine to isocyanate is 1:1.

2.3 Rheological Analysis

Changes in viscosity and storage and loss moduli (G′ and G″, respectively) during the reaction between PDMS and HDI were monitored using a rheometer (MCR302, Anton Paar). Unless otherwise stated, the measurements were performed at room temperature (25°C).

2.4 Underwater Adhesion Tests

Underwater adhesion performance was probed using a universal testing machine (model ZLC-2D, Jinan XL Testing Machinery Co., Ltd., China) equipped with a 2.5 kN load cell at a loading rate of 50 mm min^{-1}. Iron, glass, polyethylene terephthalate (PET), and polytetrafluoroethylene (PTFE) were used as substrates. Prior to testing, the adhesive (0.05 mL) was injected into a cylinder in a custom-built water-filled tank, immediately pressed with a 15 mm–diameter rod (normal load = 5 N), held for 20 s, and used to bond samples underwater. The bonded samples were cured in water at room temperature for 24 h and then subjected to tensile and lap shear adhesion tests. For lap shear tests, rectangular specimens with dimensions of 12 mm × 50 mm were used (contact area = 12 mm × 12 mm). For tensile tests, cylinders with the diameter of 15 mm (contact area = 176.7 mm^2) were used. All tests were performed in triplicate to ensure repeatability, and the results were reported as the corresponding means ± standard deviations.

3 Results and Discussion

3.1 Adhesive: Preparation and Adhesion Mechanism

The isocyanate (–N=C=O) groups of HDI reacted with the amino groups ($–NH_2$) of bis(3-aminopropyl)-terminated PDMS to form a polymeric adhesive, which had a white gel-like appearance due to the action of THF and $Ca(OH)_2$ (Fig. 1a). The residual isocyanate groups in the adhesive reacted with the hydroxyl (–OH) groups of water molecules adsorbed on the substrate to form R–NH– and R–NH–COO– structures thereon in two steps (Fig. 1b) [20–23].

$$R\text{-}N{=}C{=}O + H_2O \rightarrow R\text{-}NH_2 + CO_2 \quad (1)$$

$$R\text{-}NH_2 + \text{substrate-OH} \rightarrow \text{R-NH-substrate} + H_2O \quad (2)$$

The two-step reaction proceeds continuously and concurrently. In the first step (Eq. (1)), the isocyanate groups reacted with water to form $–NH_2$ groups and CO_2 [22]. In the second step, the thus generated $–NH_2$ groups reacted with surface hydroxyl groups to form R–NH– linkages with the substrate (Eq. (2)).

In addition, isocyanate groups reacted with surface hydroxyl groups to form R–NH–COO– linkages with the substrate (Fig. 1b, Eq. (3)) [22]:

$$R\text{-}N{=}C{=}O + \text{substrate-OH} \rightarrow \text{R-NH-COO-substrate} \quad (3)$$

Particle reinforcement can markedly enhance adhesion strength [11]. Herein, $Ca(OH)_2$ reacted with the CO_2 generated according to Eq. (1) to form $CaCO_3$ particles (Eq. (4)), which exerted reinforcement effects (e.g., enhanced adhesion strength by hindering dislocation movement and altering crack propagation paths).

$$Ca(OH)_2 + CO_2 \rightarrow CaCO_3 + H_2O \quad (4)$$

Adhesive–substrate interactions included hydrogen bonding and chemical crosslinking and were expected to be substrate-dependent. For silicon-containing substrates such as glass and ceramics, –NH–COO–Si linkages may form on the surface [20], and structures such as –NH–COO–Fe, –N=Fe and –NH–Fe may form in the case of iron (Fig. 1c) [20,24]. In addition, other physical interaction may also formed, which is mainly dependent on the substrates. For example, the remaining –NH–, $–NH_2$, and C=O functional groups in the adhesive can form hydrogen bonds with the substrate surface to enhance adhesion strength [25]. As for the metal substrate like iron, $–NH_2$ can form metal complexation at the interface. The fluorine atoms of fluorinated substrates such as PTFE may interact with the hydrogen atoms in the adhesive and thus contribute to bonding van der Waals interactions.

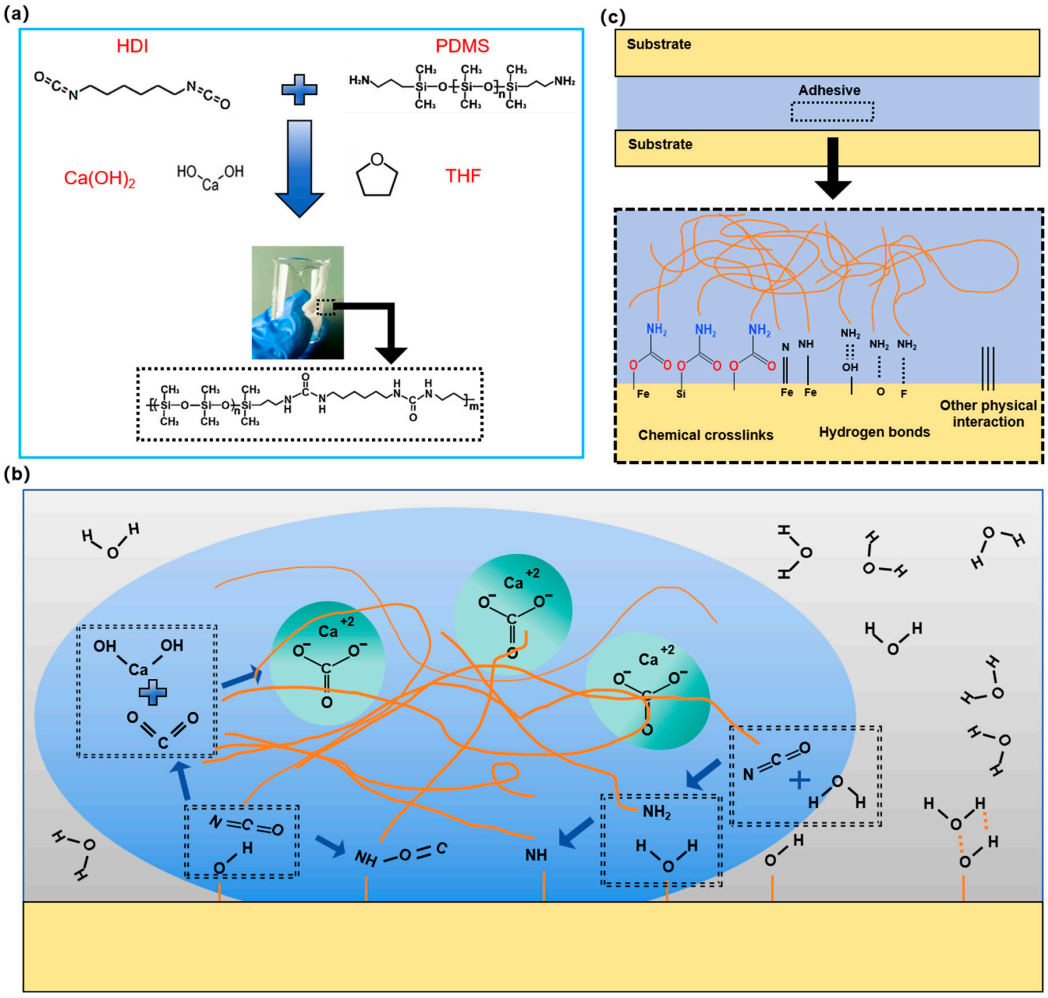

Figure 1: Schematics of (**a**) adhesive preparation, (**b**) adhesive–substrate linkage formation, and (**c**) possible interactions at the adhesive-substrate interface.

3.2 Underwater Adhesion Performance

The adhesive and rapidly cured when applied to different substrates. Once cured, the adhesive strongly adhered to glass and remained unchanged upon exposure to running water for 60 s (Fig. 2a). The adhesive demonstrated excellent adhesion to iron, silicone, glass, PET, PTFE, and copper (Fig. 2b) and rapidly. It appeared white under ambient conditions (Fig. 2c) and strongly bonded two pieces of iron when applied underwater (Fig. 2d).

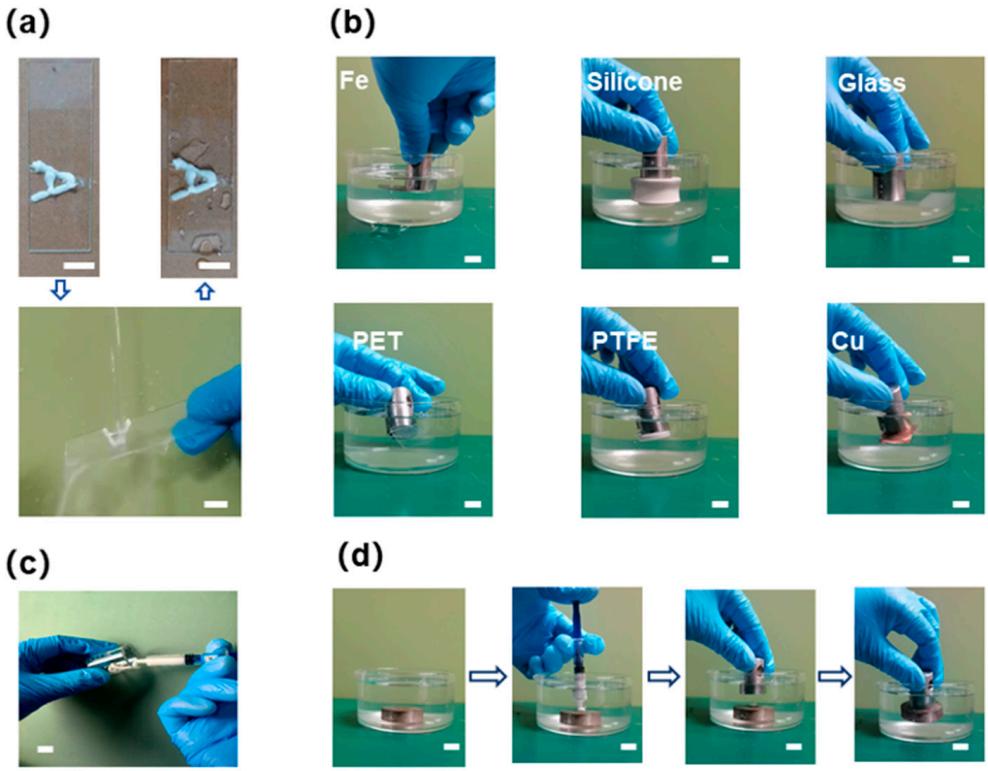

Figure 2: Illustrations showing (**a**) the impact of water flow on the glass-bonded adhesive, (**b**) the ability of the adhesive to adhere to different substrates, (**c**) the appearance of the adhesive under ambient conditions, (**d**) two iron substrates bonded together using the adhesive. The scale bar is 10 mm.

3.3 Evolution of Shear Stress and Viscosity during Adhesive Preparation

During the preparation of the adhesive, its shear stress and viscosity showed complex behavior (Fig. 3a). Both parameters increased during 0–2 s because of the effects of mixing HDI (a small-molecule monomer) with PDMS (a high-viscosity polymer). After mixing, PDMS was the main contributor to the initial viscosity because of its molecular size and polarity differing from those of HDI. The resulting phase separation caused high internal frictional resistance and hence, high shear stress.

Shear stress and viscosity rapidly decreased during 2–10 s, stabilizing during 10–73 s. The corresponding minima (37.759 Pa and 37.763 mPa s, respectively) were reached at ~41 s. This behavior was ascribed to the diffusion of HDI into PDMS. The small HDI molecules inserted between the macromolecular chains of PDMS, reducing their entanglement and internal friction and thereby decreasing system viscosity and shear stress. During this process, the reactive groups were in full contact with each other, which set the scene for the rapid subsequent increase in shear stress and viscosity due to polymerization.

After 73 s, the shear stress and viscosity rapidly increased and then stabilized, which reflected the solidification caused by the isocyanate groups of HDI extensively reacting with the hydroxyl groups of PDMS. G' and G'' remained almost unchanged during the preparation of the adhesive, which indicated that the adhesive was highly stable and could provide reliable adhesion in a constant environment (Fig. 3b).

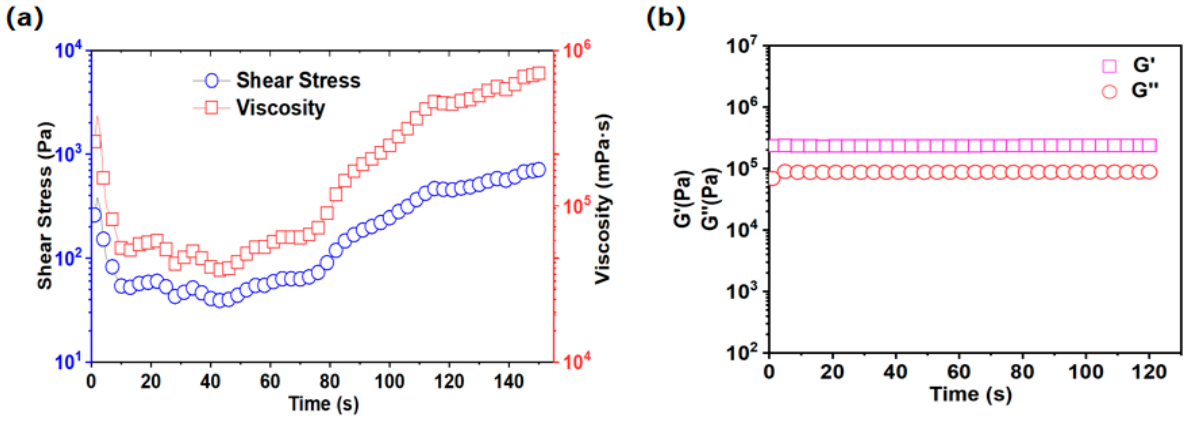

Figure 3: Evolution of (**a**) shear stress and viscosity and (**b**) storage and loss moduli (G′ and G″, respectively) during adhesive preparation at room temperature (25°C).

3.4 Effects of Various Factors on G′ and G″

We examined the responses of G′ and G″ to heating from 25°C to 100°C (Fig. 4a), cooling from 100°C to 25°C (Fig. 4b), an increase in shear strain (Fig. 4c), and an increase in frequency (Fig. 4d). G′ and G″ decreased upon heating and increased upon cooling (Fig. 4a,b). At room temperature, G′ exceeded G″, whereas the reverse was true at high temperature (100°C). Therefore, heating led to adhesion weakening [26]. As underwater adhesives are largely applied at temperatures below 100°C, the developed adhesive was concluded to be practically applicable.

Fig. 4a,b has demonstrated the thermal-responsive behavior of the adhesive. At 25°C, the values of G′ and G″ were extremely large (10^5~10^6 Pa), which is not suitable for strain and frequency-dependent measurements. Therefore, the strain and frequency-dependent measurements were performed at 65°C. Fig. 4c shows that G′ and G″ hardly changed at shear strains below 10.8% but notably decreased above this threshold. Therefore, our adhesive exhibited strong and stable adhesion at small shear strains and was deemed suitable for low-shear-strain applications. G′ and G″ increased with the increasing frequency in the range of 0.1–100 Hz (Fig. 4d). At high frequencies (>10 Hz), G′ and G″ were high. At low frequencies (<1 Hz), G′ and G″, particularly the latter, notably decreased. Therefore, our adhesive was deemed more suitable for environments with high frequencies.

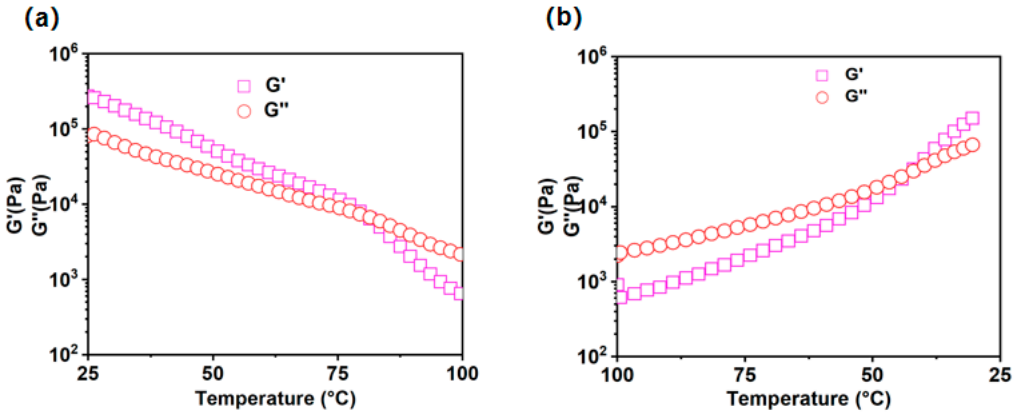

Figure 4: *Cont.*

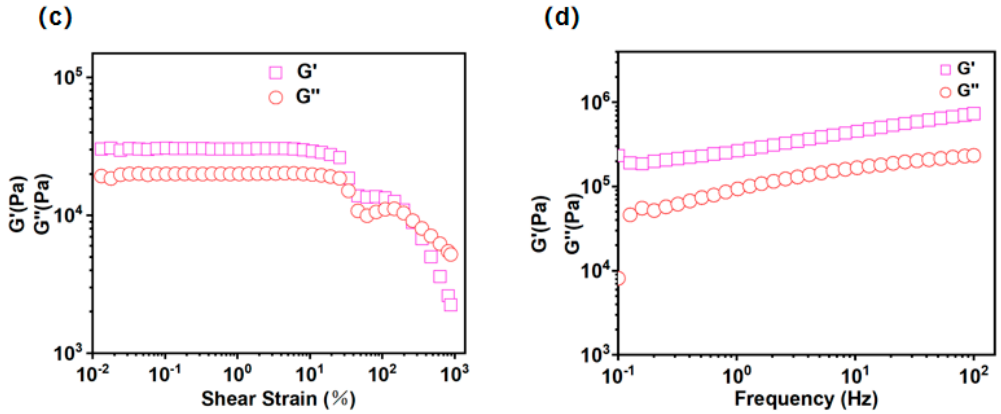

Figure 4: G′ and G″ as functions of (**a**,**b**) temperature [(**a**) heating from 25°C to 100°C, (**b**) cooling from 100°C to 25°C], (**c**) shear strain at 65°C, and (**d**) frequencies at 65°C.

3.5 Underwater Lap Shear Adhesion Test

Fig. 5a shows the setup used for lap-shear tests. Adhesion strength–displacement curves revealed that the maximum adhesion strength and adhesion strength increase rate were material-dependent (Fig. 5b). Specifically, the adhesion strength increase rate followed the order of iron > PET > glass > PTFE. The maximum adhesion strength followed the same order: iron (548 ± 44 kPa) > PET (421 ± 146 kPa) > glass (260 ± 28 kPa) > PTFE (118 ± 43 kPa) (Fig. 5c). The low maximum adhesion strength observed for PTFE was ascribed to its very low surface energy and capillary force coupled with high chemical inertness [27]. The imaging of debonded iron (Fig. 5d) and glass (Fig. 5e) samples showed that failure expectedly occurred in the adhesive and not at the adhesive–substrate interface.

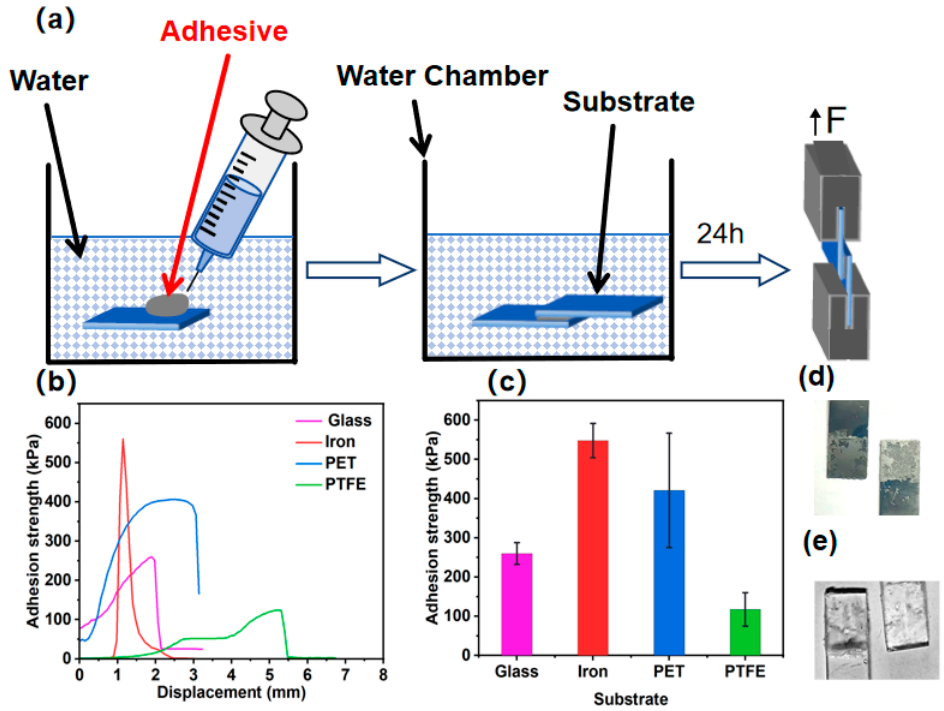

Figure 5: (**a**) Schematic of the lap shear test. (**b**) Adhesion strength–displacement curves and (**c**) maximum adhesion strengths obtained for different substrates. Images showing the adhesion failure modes of (**d**) iron and (**e**) glass.

3.6 Underwater Tensile Adhesion Test

Fig. 6a illustrates the setup used for tensile testing, with Fig. 6b,c showing the corresponding adhesion strength–displacement curves and maximum tensile strengths, respectively. The maximum tensile strength followed the order of PET (638 ± 158 kPa) > glass (416 ± 38 kPa) > iron (401 ± 24 kPa) > PTFE (227 ± 86 kPa). Notably, the shear strength exceeded the tensile strength for iron, whereas the reverse was true for the other substrates. This behavior was ascribed to the high rigidity of iron, which caused the adhesive to experience an uneven force. The high tensile adhesion strength of PET was mostly consistent with the results of the lap shear test and ascribed to the ability of this material to form numerous hydrogen bonds with the adhesive [28]. Notably, our adhesive (maximum adhesion strength = 817 kPa for PET) outperformed its recently reported counterparts [29–32] and was therefore deemed suitable for engineering applications.

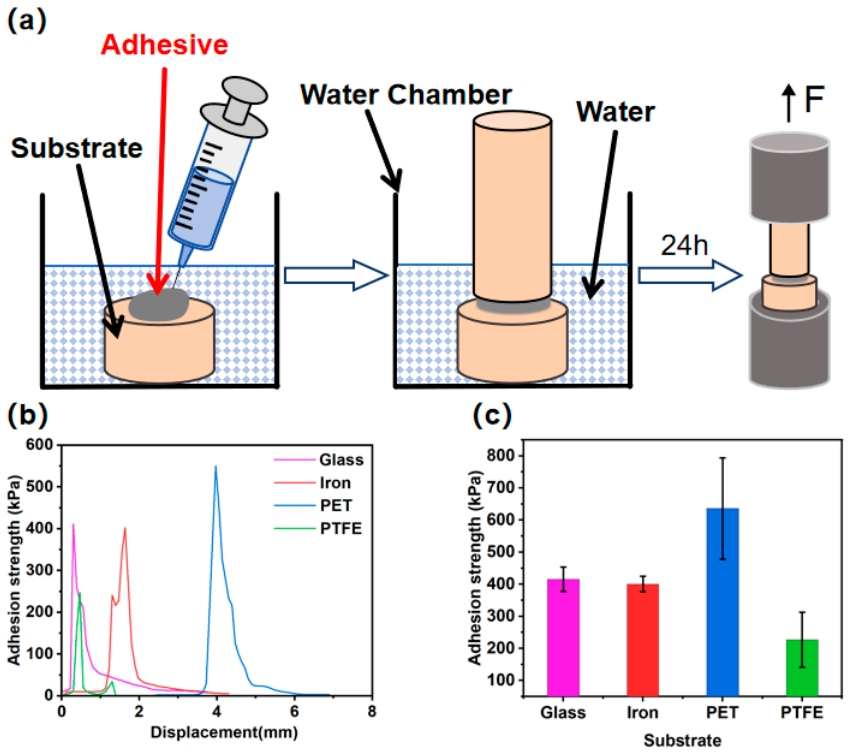

Figure 6: (**a**) Schematic of the tensile performance test. (**b**) Adhesion strength–displacement curves and (**c**) maximum adhesion strengths of various substrates.

4 Conclusion

A cheap high-performance underwater adhesive was prepared by a simple process involving the polymerization of bis(3-aminopropyl)-terminated PDMS with HDI in the presence of $Ca(OH)_2$. $Ca(OH)_2$ was used to generate particles and thus reinforce the adhesive and increase adhesion strength. After underwater curing, the adhesive exhibited strong and stable adhesion to various substrates (iron, glass, PET, and PTFE) because of the synergistic effects of particle reinforcement and interactions such as chemical crosslinking and hydrogen bonding. The maximum underwater adhesion strength was achieved for PET (817 kPa) and was sufficient to meet general application requirements. In the future, we will examine the mechanism of underwater adhesion in greater detail and develop more advanced and economical adhesives.

Acknowledgement: We would like to express our special gratitude to College of Mechanical & Electrical Engineering, Nanjing University of Aeronautics and Astronautics for their support.

Funding Statement: This work was supported by National Key R&D program of China (2023YFE0207000), Natural Science Foundation of Jiangsu Province (BK20231443).

Author Contributions: The authors confirm contribution to the paper as follows: study conception and design: Yuanchen Zhang, Linfeng Wang; data collection: Yuanchen Zhang; analysis and interpretation of results: Yuanchen Zhang, Linfeng Wang; draft manuscript preparation: Yuanchen Zhang. All authors reviewed and approved the final version of the manuscript.

Availability of Data and Materials: The data that support the findings of this study are available from the Corresponding Author, upon reasonable request.

Ethics Approval: Not applicable.

Conflicts of Interest: The authors declare no conflicts of interest.

References

1. Fan H, Gong JP. Bioinspired underwater adhesives. Adv Mater. 2021;33(44):2102983. [CrossRef].
2. Zhang C, Dou R, Xing W, Liu Q, Cai L, Xia W, et al. A novel adhesive with exceptional underwater adhesion properties, capable of complete curing in aquatic environments. J Mater Res Technol. 2024;33:8758–67. [CrossRef].
3. Li S, Sun P, Dou W, Ji W, Wang Q, Li X, et al. Water-responsive entangled underwater adhesives enable strong adhesion in natural dynamic water. Chem Eng J. 2024;479:147639. [CrossRef].
4. Wang Z, Guo L, Xiao H, Cong H, Wang S. A reversible underwater glue based on photo- and thermo-responsive dynamic covalent bonds. Mater Horiz. 2020;7(1):282–8. [CrossRef].
5. Zhao Y, Wu Y, Wang L, Zhang M, Chen X, Liu M, et al. Bio-inspired reversible underwater adhesive. Nat Commun. 2017;8:2218. [CrossRef].
6. Silverman HG, Roberto FF. Understanding marine mussel adhesion. Mar Biotechnol. 2007;9(6):661–81. [CrossRef].
7. Su X, Xie W, Wang P, Tian Z, Wang H, Yuan Z, et al. Strong underwater adhesion of injectable hydrogels triggered by diffusion of small molecules. Mater Horiz. 2021;8(8):2199–207. [CrossRef].
8. Pan F, Ye S, Wang R, She W, Liu J, Sun Z, et al. Hydrogel networks as underwater contact adhesives for different surfaces. Mater Horiz. 2020;7(8):2063–70. [CrossRef].
9. Wu J, Lei H, Fang X, Wang B, Yang G, O'Reilly RK, et al. Instant strong and responsive underwater adhesion manifested by bioinspired supramolecular polymeric adhesives. Macromolecules. 2022;55(6):2003–13. [CrossRef].
10. Stewart RJ, Ransom TC, Hlady V. Natural underwater adhesives. J Polym Sci B Polym Phys. 2011;49(11):757–71. [CrossRef].
11. Chang H, Wang J, Hu B, Wu J, Qi W, Penkova A, et al. Peptide- and protein- based underwater adhesives: lessons from marine bio-adhesion. Adv Colloid Interface Sci. 2025;346:103674. [CrossRef].
12. Saiz-Poseu J, Mancebo-Aracil J, Nador F, Busqué F, Ruiz-Molina D. The chemistry behind catechol-based adhesion. Angew Chem Int Ed. 2019;58(3):696–714. [CrossRef].
13. Hofman AH, van Hees IA, Yang J, Kamperman M. Bioinspired underwater adhesives by using the supramolecular toolbox. Adv Mater. 2018;30(19):1704640. [CrossRef].
14. Yang S, Ma Y, Qin C, Zhang Z, Yu J, Pei X, et al. Light-controlled switchable underwater adhesive. SmartMat. 2024;5(2):e1235. [CrossRef].
15. Lee H, Ryu Y, Oh Y, Kim C, Lee Y, Choi H, et al. Starfish-inspired tube feet for temporary and switchable underwater adhesion and transportation. Sci Adv. 2025;11(30):eadx3539. [CrossRef].
16. Zhu NX, Wei ZW, Chen CX, Wang D, Cao CC, Qiu QF, et al. Self-generation of surface roughness by low-surface-energy alkyl chains for highly stable superhydrophobic/superoleophilic MOFs with multiple functionalities. Angew Chem. 2019;131(47):17189–96. [CrossRef].

17. Cui X, Liu J, Xie L, Huang J, Liu Q, Israelachvili JN, et al. Modulation of hydrophobic interaction by mediating surface nanoscale structure and chemistry, not monotonically by hydrophobicity. Angew Chem. 2018;130(37):12079–84. [CrossRef].
18. Zeng H, Xie Q, Ma C, Zhang G. Silicone elastomer with surface-enriched, nonleaching amphiphilic side chains for inhibiting marine biofouling. ACS Appl Polym Mater. 2019;1(7):1689–96. [CrossRef].
19. Yan Y, Huang J, Qiu X, Zhuang D, Liu H, Huang C, et al. A strong underwater adhesive that totally cured in water. Chem Eng J. 2022;431:133460. [CrossRef].
20. Zhang G, Dass A, Rawashdeh AM, Thomas J, Counsil JA, Sotiriou-Leventis C, et al. Isocyanate-crosslinked silica aerogel monoliths: preparation and characterization. J Non Cryst Solids. 2004;350:152–64. [CrossRef].
21. Nies C, Wehlack C, Ehbing H, Dijkstra DJ, Possart W. Adhesive interactions of polyurethane monomers with native metal surfaces. J Adhes. 2012;88(8):665–83. [CrossRef].
22. Bañuls-Ciscar J, Trindade GF, Abel ML, Phanopoulos C, Pans G, Pratelli D, et al. A study of the interfacial chemistry between polymeric methylene diphenyl di-isocyanate and a Fe–Cr alloy. Surf Interface Anal. 2021;53(3):340–9. [CrossRef].
23. Suryawanshi Y, Sanap P, Wani V. Advances in the synthesis of non-isocyanate polyurethanes. Polym Bull. 2019;76(6):3233–46. [CrossRef].
24. Tardio S, Abel ML, Carr RH, Watts JF. The interfacial interaction between isocyanate and stainless steel. Int J Adhes Adhes. 2019;88:1–10. [CrossRef].
25. Steck J, Yang J, Suo Z. Covalent topological adhesion. ACS Macro Lett. 2019;8(6):754–8. [CrossRef].
26. Tang C, Li X, Li Z, Tian W, Zhou Q. Molecular simulation on the thermal stability of meta-aramid insulation paper fiber at transformer operating temperature. Polymers. 2018;10(12):1348. [CrossRef].
27. Suzuki H, Mashiko S. Measurements of adhesive forces on a polytetrafluoroethylene (PTFE) film and glass surface by mapping force curve. Thin Solid Films. 1998;331(1–2):176–80. [CrossRef].
28. Yan Y, Huang J, Qiu X, Cui X, Xu S, Wu X, et al. An ultra-stretchable glycerol-ionic hybrid hydrogel with reversible gelid adhesion. J Colloid Interface Sci. 2021;582:187–200. [CrossRef].
29. Li F, Gu W, Gong S, Zhou W, Shi SQ, Gao Q, et al. Design of amphiphilic-function-aiding biopolymer adhesives for strong and durable underwater adhesion via a simple solvent-exchange approach. Chem Eng J. 2023;469:143793. [CrossRef].
30. Cui C, Fan C, Wu Y, Xiao M, Wu T, Zhang D, et al. Water-triggered hyperbranched polymer universal adhesives: from strong underwater adhesion to rapid sealing hemostasis. Adv Mater. 2019;31(49):1905761. [CrossRef].
31. Liu H, Qin S, Liu J, Zhou C, Zhu Y, Yuan Y, et al. Bio-inspired self-hydrophobized sericin adhesive with tough underwater adhesion enables wound healing and fluid leakage sealing. Adv Funct Mater. 2022;32(32):2201108. [CrossRef].
32. Xu L, Gao S, Guo Q, Wang C, Qiao Y, Qiu D. A solvent-exchange strategy to regulate noncovalent interactions for strong and antiswelling hydrogels. Adv Mater. 2020;32(52):2004579. [CrossRef].